11/21/01 17:28 FAX 212 592 7214 NYPL EXPRESS 047

DELIVERY DESK SIBL
Nature.
no. 6630
May 15, 1997
JSM 94-543

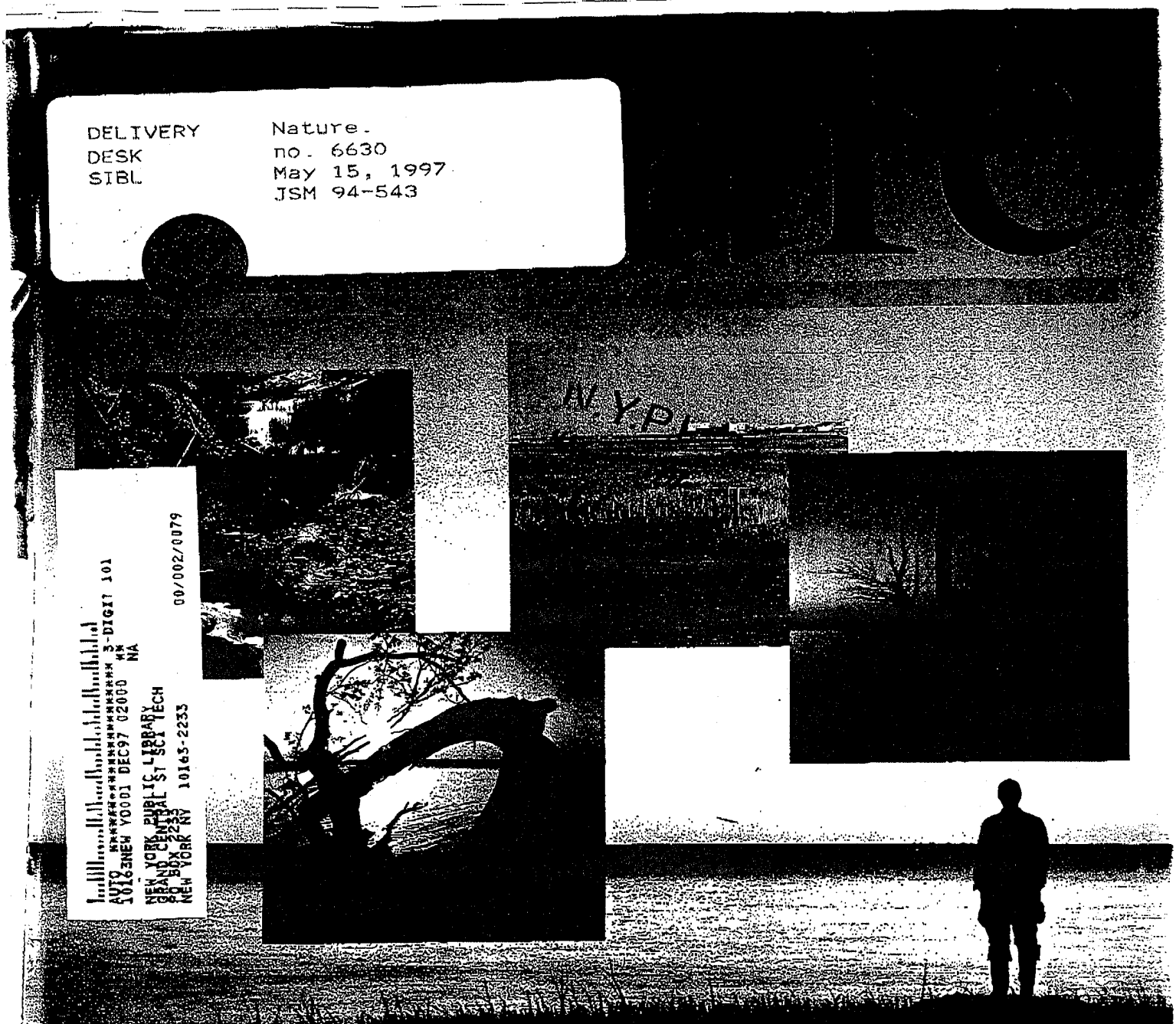

NEW YORK PUBLIC LIBRARY
SCIENCE INDUSTRY & BUSINESS LIBRARY
188 MADISON AVENUE
NEW YORK NY 10016-0122
00/002/0079

Pricing the planet

Protein unfolding The source of muscle elasticity

Callisto An undifferentiated satellite

Ocean productivity Nitrogen, the ultimate nutrient?

New on the market

book reviews

article

letters to nature

guide to authors

new on the market

classified

8. Vassar, R. *et al.* Topographic organization of sensory projections in the olfactory bulb. *Cell* 79, 981–991 (1994).
9. Ressler, K. J., Sullivan, K. L. & Buck, L. B. Information coding in the olfactory system: evidence for a stereotyped and highly organized epitope map in the olfactory bulb. *Cell* 79, 1245–1255 (1994).
10. Mombaerts, P. *et al.* Visualizing an olfactory sensory map. *Cell* 87, 675–686 (1996).
11. Boeckh, J., Distler, P., Ernst, K. D., Hösl, M. & Malun, D. in *Chemosensory Information Processing* (ed. Schild, D.) 201–227 (Springer, Berlin, 1990).
12. Firestein, S., Picco, C. & Menini, A. The relation between stimulus and response in olfactory receptor cells of the tiger salamander. *J. Physiol.* 468, 1–10 (1993).
13. Schild, D. Signal integration in the olfactory system. *Trends Neurosci.* 17, 366–367 (1994).
14. Christensen, T. A., Waldrop, B. R., Harrow, I. D. & Hildebrand, J. G. Local interneurons and information processing in the olfactory glomeruli of the moth *Manduca sexta*. *J. Comp. Physiol. A* 173, 385–399 (1993).
15. Sun, X., Fonta, C. & Masson, C. Odour quality processing by bee antennal lobe interneurons. *Chem. Senses* 18, 555–577 (1993).
16. Mori, K. & Yoshihara, Y. Molecular recognition and olfactory processing in the mammalian olfactory system. *Progr. Neurobiol.* 45, 585–619 (1995).
17. Wehr, M. & Laurent, G. Odour encoding by temporal sequences of firing in oscillating neural assemblies. *Nature* 384, 162–166 (1996).
18. Flanagan, D. & Mercer, A. R. An atlas and 3-D reconstruction of the antennal lobes in the worker honey bee, *Apis mellifera*. *Int. J. Insect Morphol. Embryol.* 18, 145–159 (1989).
19. Christensen, T. A., Hildebrand, J. G., Tumlinson, J. H. & Doolittle, R. E. Sex pheromone blend of *Manduca sexta*: responses of central olfactory interneurons to antennal stimulation in male moths. *Arch. Insect Biochem. Physiol.* 10, 281–291 (1989).
20. Tank, D. W., Gelperin, A. & Kleinfeld, D. Odors, oscillations, and waves: does it all compute? *Science* 265, 1819–1820 (1994).
21. Hansson, B. S., Ljungberg, H., Hallberg, E. & Löfstedt, C. Functional specialization of olfactory glomeruli in a moth. *Science* 256, 1313–1315 (1992).
22. Pelz, C., Gerber, H. & Menzel, R. Odorant intensity as a determinant for olfactory conditioning in honeybees: roles in discrimination, overshadowing and memory consolidation. *J. Exp. Biol.* 200, 837–847 (1997).
23. Yuste, R. & Katz, L. C. Control of postsynaptic Ca^{++} influx in developing neocortex by excitatory and inhibitory neurotransmitters. *Neuron* 6, 333–344 (1991).
24. O'Donovan, M. J., Ho, S., Sholomenko, G. & Yee, W. Realtime imaging of neurons retrogradely and anterogradely labelled with calcium-sensitive dyes. *J. Neurosci. Meth.* 46, 91–106 (1993).
25. Akers, R. P. & Getz, W. M. Response of olfactory receptor neurons in honey bees to odorants and their binary mixtures. *J. Comp. Physiol. A* 173, 169–185 (1993).
26. Distler, P. GABA-immunohistochemistry as a label for identifying types of local interneurons and their synaptic contacts in the antennal lobes of the american cockroach. *Histochemistry* 93, 617–626 (1990).
27. Hansson, B. S., Anton, S. & Christensen, T. A. Structure and function of antennal lobe neurons in the male turnip moth, *Agrotis segetum*. *J. Comp. Physiol. A* 175, 547–562 (1994).
28. Ache, B. W. Towards a common strategy for transducing olfactory information. *Semin. Cell Biol.* 5, 55–63 (1994).
29. Hammer, M. & Menzel, R. Learning and memory in the honeybee. *J. Neurosci.* 15, 1617–1630 (1995).
30. Kendrick, K. M., Levy, F. & Keverne, E. B. Changes in the sensory processing of olfactory signals induced by birth in sheep. *Science* 256, 833–836 (1992).
31. Friedrich, R. W. & Katsching, S. I. *Neuron* 833–836 (in the press).

Acknowledgements. We thank M. Hammer, M. Glurfa, R. Yuste and A. Borst for helpful comments on the manuscript and B. Corvette for help with the English. We are grateful to T. Faber for experimental support and to S. McIlwrath for providing the preparation of the antennal lobe shown in Fig. 1A,a.

Correspondence and requests for materials should be addressed to J.J. (e-mail: joerges@neurobiologie.fu-berlin.de).

Presenilin 1 is required for *Notch1* and *Dll1* expression in the paraxial mesoderm

Philip C. Wong*†#, Hui Zheng‡#, Hua Chen*†, Mark W. Becher*†, Dalip J. S. Sirinathsinghji§, Myrna E. Trumbauer‡, Howard Y. Chen‡, Donald L. Price*†‖¶, Lex H. T. Van der Ploeg‡ & Sangram S. Sisodia*†‖

*Departments of * Pathology, ‖ Neuroscience and ¶ Neurology, and † the Neuropathology Laboratory, The Johns Hopkins University School of Medicine, Baltimore, Maryland 21205, USA*
‡ Department of Genetics and Molecular Biology, Merck Research Laboratories, Rahway, New Jersey 07065, USA
§ Merck Sharp and Dohme Research Laboratories, Neuroscience Research Center, Terlings Park, Eastwick Road, Essex CM20 2QR, UK
 # These authors contributed equally to this work.

Approximately 10% of cases of Alzheimer's disease are familial and associated with autosomal dominant inheritance of mutations in genes encoding the amyloid precursor protein[1], presenilin 1 (PS1)[2] and presenilin 2 (PS2)[3,4]. Mutations in *PS1* are linked to about 25% of cases of early-onset familial Alzheimer's disease[5]. PS1, which is endoproteolytically processed *in vivo*[6], is a multipass transmembrane protein and is a functional homologue of SEL-12 (ref. 7), a *Caenorhabditis elegans* protein that facilitates signalling mediated by the Notch/LIN-12 family of receptors[8,9]. To examine potential roles for PS1 in facilitating *Notch*-mediated signalling during mammalian embryogenesis, we generated mice with targeted disruptions of *PS1* alleles (*PS1*$^{-/-}$ mice). *PS1*$^{-/-}$ embryos exhibited abnormal patterning of the axial skeleton and spinal ganglia, phenotypes traced to defects in somite segmentation and differentiation. Moreover, expression of mRNA encoding Notch1 and Dll1 (delta-like gene 1)[10], a vertebrate Notch ligand, is markedly reduced in the presomitic mesoderm of *PS1*$^{-/-}$ embryos compared to controls. Hence, PS1 is required for the spatiotemporal expression of *Notch1* and *Dll1*, which are essential for somite segmentation and maintenance of somite borders[11–13].

In the *PS1* targeting construct, an ~1.9 kilobase fragment containing the second coding exon (exon 4, amino acids 30–113) and flanking intronic segments of the *PS1* gene was replaced by a neomycin-resistance gene (Fig. 1a). The linearized targeting vector was electroporated into AB2.1 embryonic stem (ES) cells and two ES cell lines (from a total of 65 clones) with a single targeted allele were used for the generation of *PS1*$^{-/-}$ mice. Genotyping of

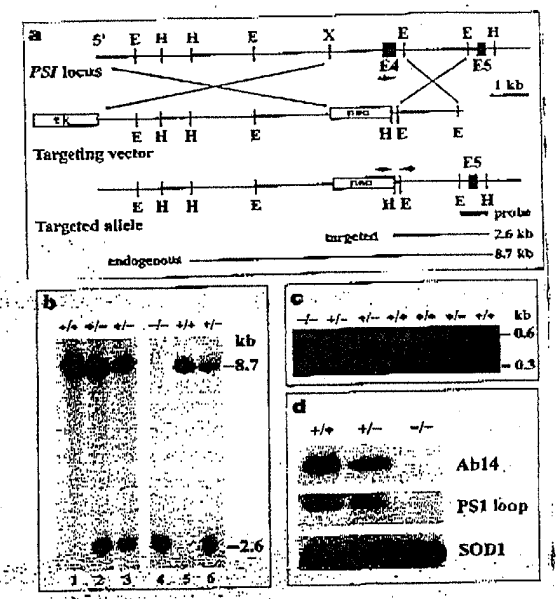

Figure 1 Targeted disruption of the *PS1* gene by homologous recombination. **a**, Maps of the wild-type *PS1* locus, the targeting vector, and the disrupted *PS1* allele. Exons 4 and 5 of *PS1* are indicated by black boxes. The targeting vector shows the replacement of exon 4 and flanking genomic sequences by the neomycin gene (neo) and the HSV thymidine kinase gene (tk). Arrows indicate the sites within the targeted and wild-type *PS1* alleles from which PCR primers were chosen for genotyping. Lines below denote expected sizes for *Hin*dIII-digested fragments detected with a 3′-flanking probe (black bar) from targeted and endogenous *PS1* alleles. E, *Eco*RI; H, *Hin*dIII; X, *Xba*I. **b**, Analysis of genomic DNA from ES cells (1, wild type; 2, clone 300; 3, clone 688; and embryos from *PS1*$^{+/-}$ crosses (lanes 4–6; genotypes for the *PS1* targeted allele are indicated above the lanes). The *Hin*dIII fragments detected for wild-type (8.7 kb) and targeted (2.6 kb) *PS1* alleles with the 3′ probe are indicated. **c**, PCR analysis of DNA extracted from yolk sac. Using primers indicated in **a**, the 370-bp or 500-bp fragment is specific to the targeted or endogenous *PS1* allele respectively. **d**, Total protein extracts (100 μg) of wild-type (+/+), heterozygous (+/−) and homozygous PS1 knockout (−/−) E18.5 embryos were immunoblotted using rabbit polyclonal antisera specific for epitopes in the N terminus (Ab14) and the loop region (PS1 loop) of PS1, and superoxide dismutase 1 (SOD1). Bound antibodies were detected with ^{125}I-labelled protein A.

Payment has been made to the Copyright Clearance Center for this article

PS1$^{-/-}$ mice were performed by DNA blotting (Fig. 1b) and polymerase chain reaction (PCR) methods (Fig. 1c). To confirm that the targeting event led to inactivation of the *PS1* gene, we prepared total SDS extracts from embryos at embryonic day 18.5 (E18.5) and subjected these preparations to immunoblotting analysis with antibodies specific for epitopes contained within each of the endoproteolytic products of PS1 that normally accumulate *in vivo*[6]. In *PS1*$^{+/-}$ mice, PS1 derivatives accumulate to ~50% the level of control littermates, whereas *PS1*$^{-/-}$ mutant mice showed no evidence of accumulation of PS1-related polypeptides (Fig. 1d). These results confirmed the targeted inactivation of *PS1*.

Although no homozygous mutant mice survived beyond the first day after birth (>50 litters examined), *PS1*$^{-/-}$ embryos were present at expected mendelian frequencies at various stages of

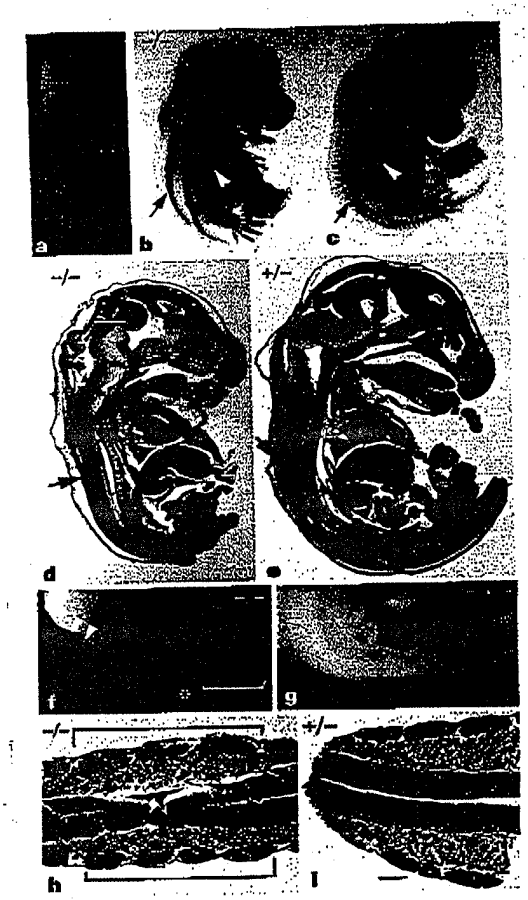

Figure 2 Abnormal patterning of the axial skeleton and somite segmentation defect in *PS1*$^{-/-}$ embryos. **a**, E17.5 embryos were fixed and photographed intact; note the overall size reduction and the stubby tail of the *PS1*$^{-/-}$ embryo (top) compared to a littermate control (bottom). **b**, **c**, Skeletal preparations of alcian blue (cartilage) stained *PS1*$^{-/-}$ (**b**) and *PS1*$^{+/+}$ (**c**) E13.5 embryo. Note the vertebral rudiments are fused (arrow) and rib formation (arrowhead) is defective in *PS1*$^{-/-}$ embryo (**b**), whereas the vertebral column (arrow) and ribs (arrowhead) in littermate control (**c**) are orderly segmented. **d**, **e**, Sagittal section of E15.5 *PS1*$^{-/-}$ embryo (**d**) shows abnormal segmentation of vertebral column (bracket) adjacent to spinal cord (s) and fusion of dorsal arches (large arrow) compared to *PS1*$^{+/-}$ control (**e**). Note the severe bending of the basioccipital bone (small arrow) and the downward disposition of the hindbrain and brainstem in the *PS1*$^{-/-}$ (**d**) compared to the *PS1*$^{+/-}$ (**e**) embryo. The arrowhead denotes the distorted angle formed between the basioccipital bone and the atlas in the *PS1*$^{-/-}$ (**d**) compared to the *PS1*$^{+/-}$ (**e**) embryo. **f**, **g**, *PS1*$^{-/-}$ (**f**) and *PS1*$^{+/-}$ (**g**) E9.5 embryos were fixed and photographed intact. An ordered array of somites is apparent in *PS1*$^{+/-}$ embryos (**g**), whereas some somites in *PS1*$^{-/-}$ embryos (**f**) appear compressed (arrowheads) and fused (asterisks); note the unsegmented condensation of somites (bracketed in **f**). **h**, **i**, Somite segmentation in *PS1*$^{+/-}$ (**i**) embryos is coordinated across the midline, whereas asymmetric segmentation of somites is observed in *PS1*$^{-/-}$ embryo (**h**). Scale bar, 100 μm.

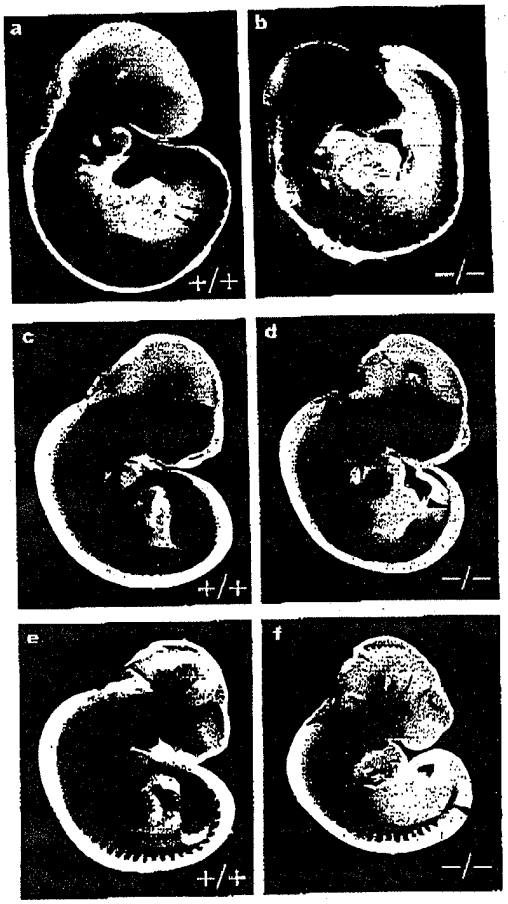

Figure 3 Expression patterns of somitic lineage genes in wild-type and *PS1*$^{-/-}$ embryos. Detection of *paraxis* (**a**, **b**), *Pax-1* (**c**, **d**) and *myogenin* (**e**, **f**) mRNAs by whole-mount *in situ* hybridization of E9.5 (**a**, **b**) and E10.5 (**c**–**f**) embryos. Controls (**a**, **c** and **e**) and *PS1*$^{-/-}$ (**b**, **d** and **f**) embryos are shown. Note the regular staining pattern indicated by arrows in the control embryo in **a**, the irregular pattern of staining (arrowheads) in somites of mutant embryo in **b**, the segmented staining pattern (arrow) in the control embryo in **c**, the unsegmented staining pattern in the caudal region of *PS1*$^{-/-}$ embryo (arrowhead) in **d**, the metameric staining pattern denoted by the arrow in the control embryo in **e**, and the unevenly spaced and fused staining pattern in the caudal region of the mutant embryo (arrowhead) in **f**.

gestation from E8.5 to E18.5 (>50 litters examined). We have not yet observed any developmental deficits in mice with a heterozygous mutation of *PS1*. The most striking phenotype observed in $PS1^{-/-}$ embryos was a severe perturbation in the development of the axial skeleton. Compared to controls, $PS1^{-/-}$ mutant embryos (E10 to E18) are smaller and possess a stubby tail (Fig. 2s). Histochemical analysis of the skeleton of $PS1^{-/-}$ E13.5 embryos, using alcian blue stain, revealed considerable defects in the formation of vertebral column and ribs (Fig. 2b,c), although the limbs appeared normal. In mid-sagittal sections from E15.5 $PS1^{-/-}$ embryos, we observed that the vertebral column is drastically shortened and fails to undergo proper segmentation(Fig. 2d,e).

The metameric pattern of the axial skeleton, a structure derived entirely from cells in the ventral halves of the somites, is predetermined during somitogenesis[14,15]. During somite differentiation, cells from the ventral compartment of somites form the mesenchymal sclerotomes, which eventually give rise to vertebral bodies, intervertebral discs, neural arches, pedicles and ribs[14]. To determine whether somitogenesis is affected in $PS1^{-/-}$ embryos, we examined embryos between E8.5 and E10.5, when somites are being generated. From intact E9.5 $PS1^{-/-}$ embryos, we observed irregularly shaped somites along the entire length of the neural tube, although somites were largely absent at the caudalmost regions (Fig. 2f). Further histological examination of E9.5 $PS1^{-/-}$ embryos revealed misalignment of somites (Fig. 2h) compared to wild-type embryos in which somites are in tight register across the midline (Fig. 2i). These abnormal somite patterns in $PS1^{-/-}$ embryos are highly reminiscent of somite segmentation defects described in mice with functionally inactivated *Notch1* (ref. 11) or *Dll1* (ref. 13) alleles.

To examine somite differentiation in $PS1^{-/-}$ embryos, we used whole-mount *in situ* hybridization to analyse the expression of genes that identify specific somitic lineages. *Paraxis*, a gene encoding a basic helix–loop–helix (bHLH) transcription factor, is normally expressed highly in paraxial mesoderm and in newly formed somites[16]. In contrast to wild-type E9.5 embryos, in which *Paraxis* is expressed in the entire rostrocaudal array of somites (Fig. 3a), the staining pattern in somites of $PS1^{-/-}$ embryos is highly disorganized and irregular (Fig. 3b). *Pax-1*, a gene of the paired box transcription factor family, is specifically expressed in sclerotomal cells in the ventral portion of the somites[17,18]. In E10.5 $PS1^{+/+}$ embryos, *Pax-1* is expressed in a segmented array throughout the ventral sclerotome (Fig. 3c). Although the rostral ventral sclerotome of $PS1^{-/-}$ embryos exhibit strong *Pax-1* expression, the staining becomes continuous without defined boundaries in the caudal region beginning at the hind limb-bud level (Fig. 3d). *Myogenin*, a bHLH transcription-factor gene specific to the myogenic lineage, is normally expressed in a metameric pattern along the craniocaudal axis in the myotome[19]. Although the characteristic metameric staining pattern of *myogenin* in the rostral portion of E10.5 $PS1^{-/-}$ embryos is similar to that of control embryos (Fig. 3e,f), *myogenin* expression is considerably reduced and the boundaries are not as sharply defined in the caudal region of the mutant embryo (Fig. 3f). These analyses show that, despite the clear disruption in somite segmentation in $PS1^{-/-}$ embryos, specification of somitic cell lineages, particularly the sclerotome and dermomyotome, is apparently unaffected.

In view of the similarities in somite segmentation defects in $PS1^{-/-}$ embryos and embryos with functionally inactivated *Notch1* (ref. 11) or *Dll1* (ref. 13) alleles, we examined the expression of *Notch1* and *Dll1* mRNA in $PS1^{-/-}$ embryos. At E8.5 and E9.5, the abundant expression of *Notch1* mRNA observed in the presomitic mesoderm of control embryos (Fig. 4a,c) is nearly abolished in the $PS1^{-/-}$ embryos (Fig. 4b,d). Analysis of *Dll1* mRNA expression show that, although high levels of *Dll1* mRNAs are observed in the presomitic mesoderm of E9.5 control embryos (Fig. 4c), the levels are markedly reduced in $PS1^{-/-}$ embryos (Fig. 4f). We confirmed that *PS1* mRNAs are also expressed in the presomitic mesoderm and somites in wild-type embryos (Fig. 4g), albeit at significantly lower levels than *Notch1* and *Dll1*. These data suggest that PS1 regulates the spatiotemporal expression of *Notch1* and *Dll1* in the paraxial mesoderm. However, the mechanisms by which PS1 influences extrinsic or intrinsic signalling pathways necessary for cell-autonomous amplification of *Notch1* or *Dll1* mRNA in the presomitic mesoderm[8,11] remain to be established.

Because *Dll1* is required for the maintenance of somite borders, such that segment polarity is established in each somite[13], we examined whether somite polarity is maintained in $PS1^{-/-}$ embryos. Histological analysis of $PS1^{-/-}$ E11.5 embryos revealed that sclerotome condensation failed to occur (Fig. 4h), suggesting that the identity of the caudal halves of each segment were not specified. As a test of this model we examined the morphogenesis of

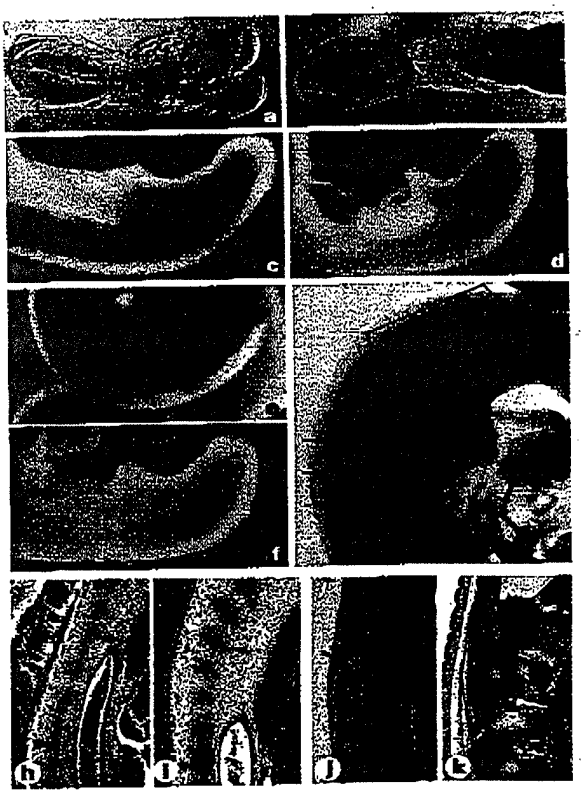

Figure 4 Reduced expression of *Notch1* and *Dll1*, abnormal sclerotome differentiation, and spinal ganglia patterning defects in $PS1^{-/-}$ embryos. **a–d**, Detection of *Notch1* mRNA by whole-mount *in situ* hybridization of E8.5 (**a**, **b**) and E9.5 (**c**, **d**) embryos. Note the reduction of *Notch1* signals in $PS1^{-/-}$ embryos in the presomitic mesoderm (indicated by brackets). **e**, **f**, Detection of *Dll1* mRNA by whole-mount *in situ* hybridization of E9.5 embryos. Note the decreased *Dll1* signal in $PS1^{-/-}$ embryo in the presomitic mesoderm (indicated by bracket). **g**, Detection of PS1 mRNA by whole-mount *in situ* hybridization of E9.5 embryos. Arrows point to the somites and bracket denotes the presomitic mesoderm. Control (**a**, **c**, **e**, **g**) and $PS1^{-/-}$ (**b**, **d**, **f**) mice are shown. **h**, **i**, Sclerotome of $PS1^{-/-}$ (**h**) and $PS1^{+/-}$ (**i**) embryos at E11.5. The arrow in **b** points to the condensation of sclerotomic material in the $PS1^{+/-}$ embryo, whereas the intrasegmental condensation (arrow in **a**) has not occurred in the $PS1^{-/-}$ embryo; arrowhead, notochord; s, spinal cord. **j**, **k**, Parasagittal section of E15.5 $PS1^{-/-}$ embryo (**j**) showing fusion of DRG, denoted by an asterisk; the arrow points to the non-segmented axial skeleton. DRG, indicated by an asterisk, are segmented in E15.5 $PS1^{+/-}$ embryo (**k**). Sections in **h**–**k** were stained with haematoxylin and eosin. Scale bars: **h**, **i**, 200 μm; **j**, **k**, 100 μm.

the dorsal root ganglia (DRG). Classical somite transplantation experiments in chick–quail chimaeric embryos[20,21] demonstrated that morphogenesis of DRG is intimately governed by the craniocaudal differentiation of individual somites. In *PS1*$^{-/-}$ embryos, the DRG were fused over multiple segments along the craniocaudal axis of the vertebral column (Fig. 4j,k), strongly suggesting that somite segment polarity is disrupted. Moreover, recent studies[13] have demonstrated that *Dll1*-null embryos also show abnormal condensation of sclerotome and fused DRG. These data, taken together with our observation that *Dll1* mRNA is severely reduced in the presomitic mesoderm of *PS1*$^{-/-}$ embryos (Fig. 4f), lead us to conclude that PS1 is essential for the function of Dll1 in establishing somite borders and segment polarity.

Although the cellularity and cytoarchitecture of the developing brain of *PS1*$^{-/-}$ embryos appeared normal, all *PS1*$^{-/-}$ embryos after E11.5 exhibited haemorrhages that were limited to the brain (Fig. 5a) and/or spinal cord (data not shown); these lesions were not seen in *PS1*$^{+/-}$ or *PS1*$^{+/+}$ littermates. The severity of the haemorrhages varied between individual embryos, and seemed to correlate with morbidity (assessed by lack of heartbeat). The haemorrhages are present beneath the primordial dura and leptomeninges, within the ventricles, and in neural parenchyma, rarely with focal necrosis (Fig. 5b). Taken together with the demonstration that haemorrhages in the central nervous system (CNS) are consistently observed in mice with functionally ablated *Dll1* (ref. 13) and *Jagged* (T. Gridley, personal communication) genes, these studies offer support for the view that the encoded molecules facilitate Notch signalling pathways in the development of the CNS vasculature.

Despite our demonstration that PS1 is essential for mouse embryonic development, the function(s) of PS1 during maturation and ageing is not clear, although PS1 is also expressed throughout the adult life of rodents and humans[2,22,23]. However, autosomal dominant forms of early-onset familiar Alzheimer's disease are linked to mutations in PS1 and, by mechanisms presently unclear, mutant PS1 enhances the production of highly amyloidogenic Aβ42 peptides both *in vitro* and *in vivo*[24–26]. These studies suggest that one mechanism by which mutant PS1 predisposes individuals to Alzheimer's disease is by the gain of a deleterious function. Together with the identification of missense mutations in *Notch3* in pedigrees with CADASIL, a disorder characterized by stroke and dementia[27] these results suggest that, although perturbations in Notch signalling pathways in embryos lacking genes encoding PS1, Notch or ligands of Notch lead to developmental loss-of-function disorders, mutations in these genes lead to autosomal dominant disorders associated with dementia in adult life. □

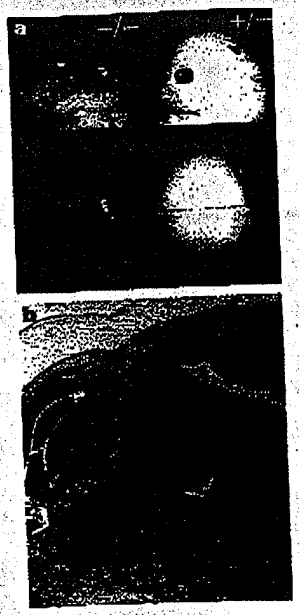

Figure 5 Central nervous system haemorrhage. **a**, A marked brain haemorrhage is evident in the *PS1*$^{-/-}$ (top left (side view) and bottom left (top view)) compared to the *PS1*$^{+/+}$ (top right (side view) and bottom right (top view)) intact E15.5 embryo. **b**, Haemorrhage occurs within ventricles (asterisk), connective tissue overlying the brain (primitive leptomeninges; arrowhead) and parenchyma (arrow). Scale bar, 200 μm.

Methods

Gene targeting of *PS1* gene. Genomic clones containing exon 4 of mouse *PS1* were isolated from a 129/Sv strain of mouse (Lambda FIX II Library, Stratagene, La Jolla, CA). We replaced a 1.9-kb *XhoI/EcoRI* fragment containing exon 4 with the neomycin phosphotransferase gene under the control of the PGK promoter. Introduction of a negative selection marker, the herpes simplex virus thymidine kinase gene, at the 5′ end of the construct allowed the use of the positive and negative selection scheme[28]. The targeting vector was linearized at a unique *BamHI* site before transfection into AB2.1 ES cells, which were subject to double selection, as previously described[29]. Clones were picked and expanded, and DNA was isolated from a portion of the cells and screened by Southern blot analysis. Frozen cells were expanded and injected into C57B1/6J blastocytes.

Histology and *in situ* RNA analysis. Embryos were fixed in 4% paraformaldehyde for 2 h at 27 °C, dehydrated, embedded in paraffin and sectioned at 10 μm. Sections were stained with either haematoxylin and eosin or Masson trichrome for histological analysis. Cartilages of embryos were stained with alcian blue[30]. For RNA detection, embryos were first genotyped by allele specific PCR of yolk-sac DNA and then subjected to whole-mount *in situ* hybridization[30].

Received 1 April; accepted 21 April 1997.

1. Busfield, F. & Goate, A. M. in *Pathology of Alzheimer's Disease*, 59–75 (Academic, San Diego, 1995).
2. Sherrington, R. *et al.* Cloning of a gene bearing missense mutations in early-onset familial Alzheimer's disease. *Nature* 375, 754–760 (1995).
3. Levy-Lahad, E. *et al.* Candidate gene for the chromosome 1 familial Alzheimer's disease locus. *Science* 269, 973–977 (1995).
4. Rogaev, E. I. *et al.* Familial Alzheimer's disease in kindreds with missense mutations in a gene on chromosome 1 related to the Alzheimer's disease type 3 gene. *Nature* 376, 775–778 (1995).
5. Cruts, M., Hendriks, L. & Van Broeckhoven, C. The presenilin genes: a new gene family involved in Alzheimer's disease pathology. *Hum. Mol. Genet.* 5, 1449–1455 (1996).
6. Thinakaran, G. *et al.* Endoproteolysis of presenilin 1 and accumulation of processed derivatives *in vivo*. *Neuron* 17, 181–190 (1996).
7. Levitan, D. *et al.* Assessment of normal and mutant human presenilin function in *Caenorhabditis elegans*. *Proc. Natl Acad. Sci. USA* 93, 14940–14944 (1996).
8. Artavanis-Tsakonas, S., Matsuno, K. & Fortini, M. E. Notch Signaling. *Science* 268, 225–232 (1995).
9. Levitan, D. & Greenwald, I. Facilitation of *lin-12*-mediated signalling by *tel-12*, a *Caenorhabditis elegans* S182 Alzheimer's disease gene. *Nature* 377, 351–354 (1995).
10. Bettenhausen, B. *et al.* Transient and restricted expression during mouse embryogenesis of *Dll1*, a murine gene closely related to *Drosophila Delta*. *Development* 121, 2407–2418 (1995).
11. Conlon, R. A. *et al.* *Notch1* is required for the coordinate segmentation of somites. *Development* 121, 1533–1545 (1995).
12. Swiatek, P. J. *et al.* *Notch1* is essential for postimplantation development in mice. *Genes Dev.* 8, 707–719 (1994).
13. Hrabe de Angelis, M., McIntyre II, J. & Gossler, A. Maintenance of somite borders in mice requires the *Delta* homologue *Dll1*. *Nature* 386, 717–721 (1997).
14. Verbout, A. J. The development of the vertebral column. *Adv. Anat. Embryol. Cell Biol.* 90, 1–122 (1985).
15. Christ, B. & Wilting, J. From somites to vertebral column. *Ann. Anat.* 174, 23–32 (1992).
16. Burgess, R., Cserjesi, P., Ligon, K. L. & Olson, E. N. Paraxis: a basic helix-loop-helix protein expressed in paraxial mesoderm and developing somites. *Dev. Biol.* 168, 296–306 (1995).
17. Deutsch, U., Dressler, G. R. & Gruss, P. Pax-1, a member of a paired box homologous murine gene family, is expressed in segmented structures during development. *Cell* 53, 617–625 (1988).
18. Koseki, H. *et al.* A role for *Pax-1* as a mediator of notochordal signals during the dorsoventral specification of vertebrae. *Development* 119, 649–660 (1993).
19. Montarras, D. *et al.* Developmental patterns in the expression of *Myf5*, *MyoD*, *myogenin*, and *MRF4* during myogenesis. *New Biol.* 3, 592–600 (1991).
20. Stern, C. D. & Keynes, R. J. Interactions between somite cells: the formation and maintenance of segment boundaries in the chick embryo. *Development* 99, 261–272 (1987).
21. Kalcheim, C. & Teillet, M.-A. Consequences of somite manipulation on the pattern of dorsal root ganglion development. *Development* 106, 85–93 (1989).
22. Lee, M. K. *et al.* Expression of presenilin 1 and 2 (PS1 and PS2) in human and murine tissues. *J. Neurosci.* 16, 7513–7525 (1996).
23. Kovacs, D. M. *et al.* Alzheimer-associated presenilin 1 and 2: neuronal expression in brain and localization to intracellular membranes in mammalian cells. *Nature Med.* 2, 224–229 (1996).
24. Scheuner, D. *et al.* Secreted amyloid beta-protein similar to that in the senile plaques of Alzheimer's disease is increased *in vivo* by the presenilin 1 and 2 and APP mutations linked to familial Alzheimer's disease. *Nature Med.* 2, 864–870 (1996).